Bureau of Mines Report of Investigations/1987

Rigid-Body and Elastic Solutions to Shield Mechanics

By Thomas M. Barczak

UNITED STATES DEPARTMENT OF THE INTERIOR

Report of Investigations 9144

Rigid-Body and Elastic Solutions to Shield Mechanics

By Thomas M. Barczak

UNITED STATES DEPARTMENT OF THE INTERIOR
Donald Paul Hodel, Secretary

BUREAU OF MINES
David S. Brown, Acting Director

Library of Congress Cataloging in Publication Data:

Barczak, Thomas M.
Rigid-body and elastic solutions to shield mechanics.

(Report of investigations/United States Department of the Interior, Bureau of Mines ; 9144)

Bibliography: p. 8.

Supt. of Docs. no.: I 28.23: 9144.

1. Mine roof control—Testing. 2. Longwall mining. I. Title. II. Title: Shield Mechanics. III. Series: Report of investigations (United States. Bureau of Mines) ; 9144.

TN23.U43 [TN288] 622 s [622'.334] 87-600302

CONTENTS

ILLUSTRATIONS

TABLES

UNIT OF MEASURE ABBREVIATIONS USED IN THIS REPORT

ft	foot	lb	pound
in	inch	pct	percent

RIGID-BODY AND ELASTIC SOLUTIONS TO SHIELD MECHANICS

By Thomas M. Barczak[1]

ABSTRACT

This report describes Bureau of Mines research to develop methods to evaluate loading on longwall roof supports to permit better design and more efficient utilization of these structures in compliance with the geological conditions in which they are employed. The resultant vertical and horizontal force acting on the canopy of a shield can be determined, either from a statically determinate solution assuming rigid-body mechanics and elimination of certain unknowns, or from an elastic solution by analysis of the load-displacement relationship of the shield structure. A two-dimensional rigid-body model is presented that determines resultant shield forces by measurement of leg, canopy capsule, and lemniscate link forces. An elastic solution is presented, in the form of an elastic stiffness model with two degrees of freedom, which describes the load-displacement relationship from the stiffness of the shield structure as determined in the Bureau's Mine Roof Simulator (MRS). The ability of both models to determine resultant forces acting on the shield canopy are evaluated from full-scale tests in the MRS. More advanced numerical models are also discussed as part of the Bureau's continuing effort in the evaluation of roof support structures.

[1]Research physicist, Pittsburgh Research Center, Bureau of Mines, Pittsburgh, PA.

INTRODUCTION

One of the goals of the Bureau of Mines research is to develop methods to evaluate loading on longwall roof supports to improve support design and utilization. Better design or utilization of these support structures can only be realized if their actual loading can be determined. Past efforts to evaluate the loading of longwall roof supports have generally been limited to rigid-body mechanics and static analysis of the support structure (1-2).[2] A statically determinate solution can be achieved with rigid-body mechanics only if some unknowns are eliminated. The Bureau has determined that the resultant vertical and horizontal force acting on the canopy of a longwall shield can be determined by measurement of leg, canopy capsule, and lemniscate link forces. Reaction moments and gob loading acting on the caving shield are ignored to produce a determinate solution in two dimensions.

Another approach to the solution of shield mechanics (resultant loading) is an elastic analysis of the shield structure. This analysis considers the entire shield as an elastically deformable body and determines the load-displacement relationship of this body. The Bureau has developed an elastic stiffness model with two degrees of freedom, which relates horizontal and vertical shield displacement to resultant horizontal and vertical forces acting on the canopy.

The development and limitations of rigid-body and elastic models are described in this report. The effectiveness of both models to determine horizontal and vertical shield loading are evaluated from controlled tests in the Bureau's Mine Roof Simulator (MRS) (fig. 1). A description of the MRS and its capabilities is provided in appendix A.

ACKNOWLEDGMENT

Acknowledgement is made to W. Scott Burton, former mechanical engineer, Boeing Services International, Pittsburgh, PA, who helped develop the techniques and models described in this report.

RIGID-BODY SOLUTIONS

The rigid-body solution of shield mechanics used by the Bureau assumes all components act as rigid bodies without deformation during load application. In reality, structures are never absolutely rigid and deform under the loads to which they are subjected. These deformations are usually small and do not appreciably affect the conditions of equilibrium. As such, a rigid-body solution to shield mechanics is pursued.

THREE-DIMENSIONAL MODEL

The most general evaluation of shield mechanics is to determine resultant loading (resultant forces acting on shield canopy) in three directions: vertical (roof-to-floor), horizontal (face-to-waste), and lateral (parallel to the face). Assuming forces and moments occur at each reaction point, each reaction in the shield structure is considered to have six degrees of freedom consisting of three force and three moment components. Such an analysis is indeterminate to a high degree (3). This system of equations can be reduced by combining like forces, such as left and right leg and lemniscate forces, into single equivalent force couple systems. Other reductions can be made by realistic assumptions that eliminate insignificant forces, such as lateral leg and canopy capsule forces. By proper elimination of these forces and moments, a determinate solution can be found that predicts resultant forces acting on the shield canopy in three

[2]Underlined numbers in parentheses refer to items in the list of references preceding the appendixes.

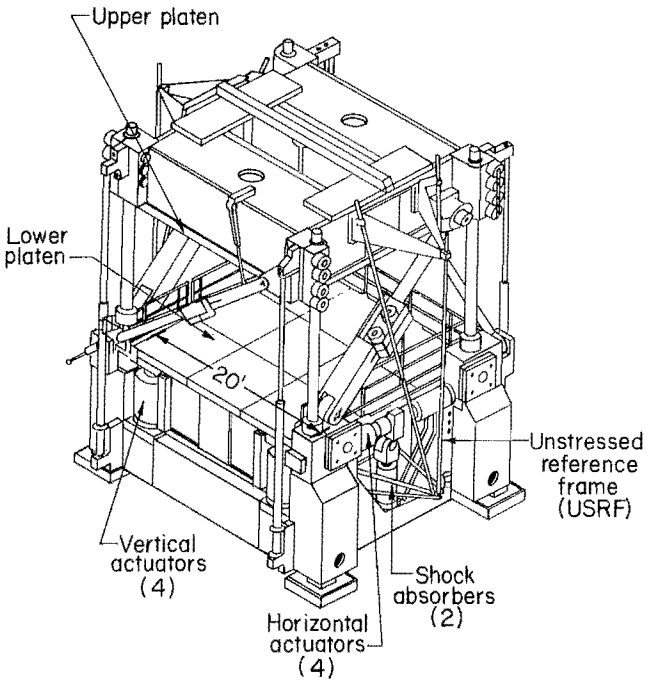

FIGURE 1.—Mine Roof Simulator.

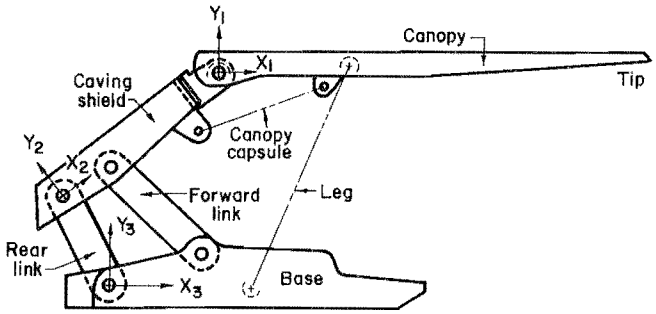

FIGURE 2.—Planar model of longwall shield support.

(vertical, horizontal, lateral) dimensions. The solution of this set of equations requires the measurement of leg, canopy capsule, and lemniscate link forces. The three-dimensional equations of equilibrium for each shield component are presented in appendix B. A complete solution to this system of equations can be found in reference 3.

TWO-DIMENSIONAL MODEL

The primary function of the shield support is to control roof-to-floor and face-to-waste strata displacements. Lateral loading parallel to the face line is not considered to be prominent in longwall mining. Hence, a two-dimensional (vertical, horizontal) analyses of shield mechanics seems appropriate.

A planar model of a two-leg shield support is illustrated in figure 2. The static equations of equilibrium can be deduced from the three-dimensional equations presented in appendix B by elimination of out-of-plane forces and moments. The two-dimensional model assumes there are no lateral (parallel to the face) loads acting on the support and does not consider the effect of moment loading due to imbalances in leg and lemniscate link forces. There is also assumed to be no gob loading, which is necessary to provide a determinate solution. Theoretical studies have shown that the presence of gob load acting on the caving shield has little impact on resultant vertical force determinations (4). The impact of gob loading on horizontal force determinations can be significant, causing errors in horizontal force determinations of about 10 to 15 pct.

The solution of the two-dimensional force determinations requires the measurement of leg, canopy capsule, and compression lemniscate link forces. These measurements can be made using a simple eight-sensor instrumentation array (fig. 3) consisting of two pressure transducers to measure leg pressures in each leg cylinder; two pressure transducers, one each to measure canopy capsule extraction and retraction pressure; and four strain gauges, two on each compression lemniscate link to measure link strain. This instrumentation array has been tested underground and found to be an effective method for determining these shield measurements (4-5).

Tests were conducted in the Bureau's MRS to evaluate the ability of the two-dimensional rigid-body model to determine resultant vertical and horizontal shield loading. The rigid-body model was found to be able to predict resultant vertical forces to within 5 pct and horizontal forces to within 25 pct in the worst case. Vertical shield load was typically predicted to within 3 pct for resultant forces acting near the leg reaction, and horizontal load predictions under most load conditions were within 10 to 15 pct

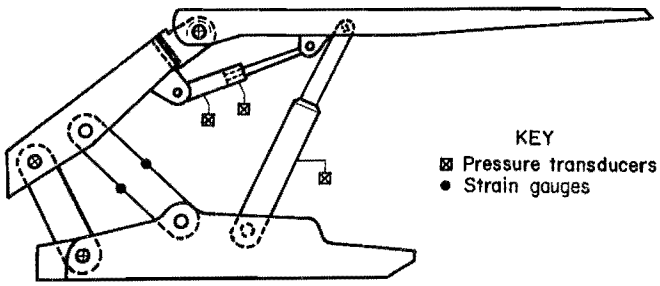

FIGURE 3.—Two-dimensional support instrumentation array.

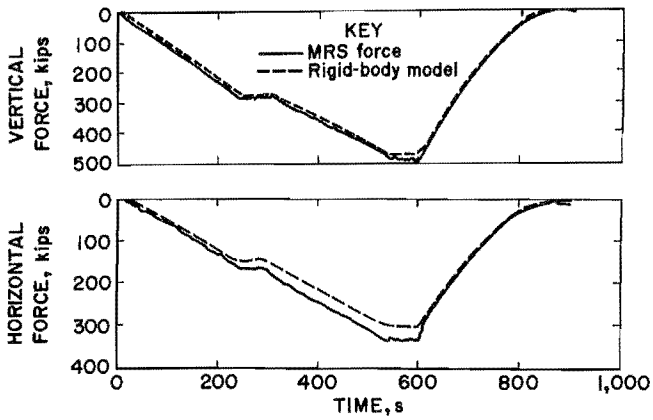

FIGURE 4.—Rigid-body model resultant vertical and horizontal force predictions.

of the applied forces. Representative examples of the rigid-body model force vertical and horizontal force predictions are shown in figure 4.

ELASTIC MODEL SOLUTIONS

The primary disadvantage of the rigid-body model is the assumptions required to produce a determinate solution. As previously indicated, several moment reactions and gob loading were eliminated to produce the determinate solution. These assumptions limit the accuracy of the model. The two-dimensional model averages imbalances in loading relative to out-of-plane forces, which also limits the capability of the model. Finally, tests have indicated that components of a typical shield support, the canopy in particular, are relatively weak in bending strength and can experience significant deformation during loading. This deformation can significantly affect the loading distribution under certain load conditions.

Theoretically, these limitations of rigid-body analysis of shield mechanics are overcome by an elastic solution where the support is considered to be a deformable body as opposed to a rigid body. If an elastic body is subjected to an external force, the body will be displaced (deformed) in proportion to the stiffness of the body (fig. 5) (3). Stiffness is a measure of the ability of a material (body) to deform and is defined as a structural engineering term as the force required to produce a unit deflection, expressed mathematically in the familiar Hooke's Law form of equation 1, where the resulting force is a linear function of the applied displacement.

$$F_X = K_X \cdot \delta, \qquad (1)$$

where F_X = uniaxial force (load),

δ = uniaxial displacement,

and K_X = uniaxial stiffness.

Therefore, if the stiffness of the body is known and the displacement measured, the resulting force can be determined.

This concept can be applied to roof supports if the support is assumed to act as an elastic body. The first requirement then is to determine the stiffness of the support. The stiffness of a longwall shield was determined from controlled displacement loading of a shield support in the MRS. Unlike the simple model presented in equation 1, where the displacement was confined to one direction, the evaluation of longwall shields must consider displacements in two directions to account for both roof-to-floor (vertical) and face-to-waste (horizontal) strata convergence (fig. 6). Therefore, an elastic model with two degrees of freedom is examined (equation 2).

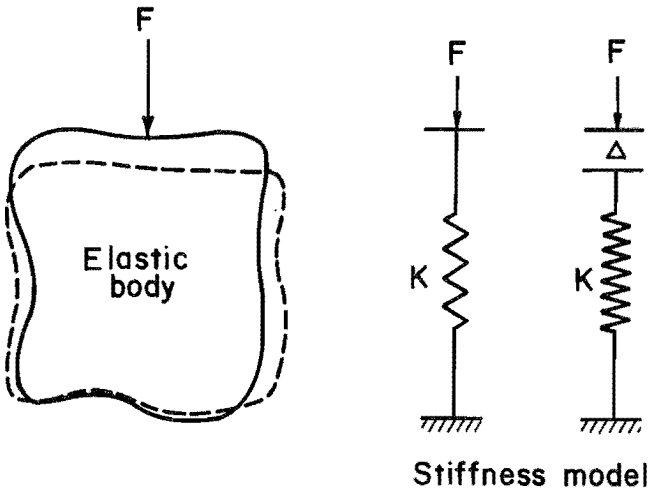

FIGURE 5.—Stiffness of an elastically deformable body.

$$F_v = K_1\delta_v + K_2\delta_h$$

and

$$F_h = K_3\delta_v + K_4\delta_h, \qquad (2)$$

where F_v = resultant vertical force,

F_h = resultant horizontal force,

δ_v = vertical displacement,

δ_h = horizontal displacement,

K_1 = vertical shield stiffness due to vertical displacement,

K_2 = vertical shield stiffness due to horizontal displacement,

K_3 = horizontal shield stiffness due to vertical displacement,

and K_4 = horizontal shield stiffness due to horizontal displacement.

The stiffness values (K_1, K_2, K_3, K_4) were determined by controlled vertical and horizontal displacement of a shield by the MRS. These stiffness tests are described in detail in appendix D. Measurement of the vertical and horizontal displacements then enable determination of the resultant vertical and horizontal forces acting on the shield canopy.

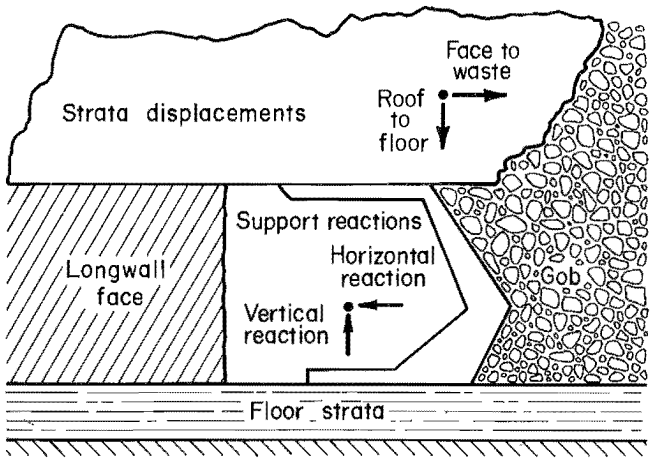

FIGURE 6.—Longwall strata displacements and support reactions.

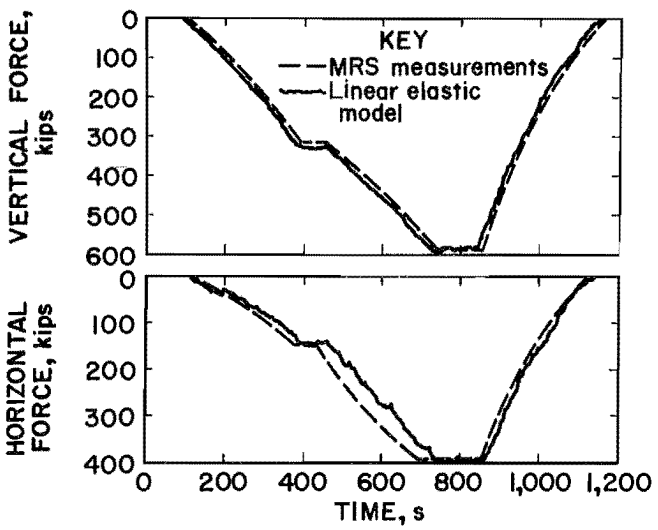

FIGURE 7.—Elastic model vertical and horizontal force predictions.

The ability of the elastic stiffness model to determine resultant shield loading is illustrated in figure 7. Vertical force predictions are very good. Horizontal force predictions are less accurate, particularly when the shield is subjected to horizontal displacements. Test results indicate some nonlinearity in the shield stiffness parameters that

produces inaccuracies in the resultant force determinations, since average stiffness coefficients were utilized in the model. Representative shield stiffness values are documented in appendix D for a typical two-legged shield support. Further studies are being pursued to evaluate the causes of the stiffness nonlinearity, but it appears that play and friction in the pin joints are largely responsible for the observed nonlinearity. The shield stiffness parameters also have been found to be functions of changes in shield geometry and setting pressures. However, if these parameters are properly considered, the elastic model is found to be an acceptable predictor of resultant shield loading.

NUMERICAL SOLUTIONS USING ELASTIC ANALYSES

The elastic analysis discussed in the previous section evaluated the support as a single deformable body. The body (support) stiffness was determined experimentally by controlled displacement loading of the support structure in the MRS. Another approach would be to determine the stiffness characteristics of each component, experimentally or numerically, and formulate a stiffness matrix from which the load-displacement relationship of the structure could be deduced from analysis of each component (6). In principal, the resultant horizontal and vertical force acting on the canopy could then be determined from measured displacements (deformations) of the shield structure.

Numerical solutions of shield mechanics can be achieved by finite-element modeling of the shield structure. The finite-element technique idealizes the support structure as a composition of a number of discrete pieces rather than as continuous elements (7). These finite elements enable the step-by-step buildup of the load-displacement relationship of a structure as a whole from those basic elements of which the structure is composed. Because the stresses are averaged over the area of the elements, the accuracy of the model is dependent, among other things, upon the number of elements.

However, the construction of finite-element models of longwall roof supports is not without difficulties. Longwall supports are basically crude pin-jointed structures, and modeling pin friction in such joints can be difficult. Other difficulties include the ability to accurately model internal platework and the effect of stress concentrations at structural discontinuities. The Bureau's experience with finite-element modeling of longwall shields is that simple models (i.e., simple beam models) constructed to fit a known shield response from physical testing, are more successful and much cheaper than complex models, which geometrically look more like the support structure, but are difficult to construct to properly simulate the structural fabrication of the shield.

Efforts to deduce load profiles from structural deformations (strain measurements) on a longwall shield from finite-element analysis have not been completely successful to date. Problems with modeling a shield structure are partially responsible, but tests and analysis have indicated that various contact configurations produce similar strain profiles in the support structure, resulting in a non-unique load-strain relationship. Therefore, multiple contact load conditions may not be predictable from finite-element analysis of the shield structure. For example, prediction of a canopy pressure (strain) distribution for a two-point canopy contact configuration from finite-element analysis of underside canopy strain contours is shown in figure 8. Resultant load predictions (i.e., single

point contact configurations) can be more accurately determined, but results to date are not better than the rigid-body and elastic shield body model presented in the previous section.

Finite-element analysis is generally used to determine stresses in a structure from applied loads. In other words, resultant loading is generally the known parameter and the deformation (displacements) are computed. Utilized in this fashion, the finite-element technique can be a valuable method to determine critical load conditions and stress concentrations in a shield structure. Such analyses can produce more efficient support designs by optimization of the distribution of stresses in the support structure.

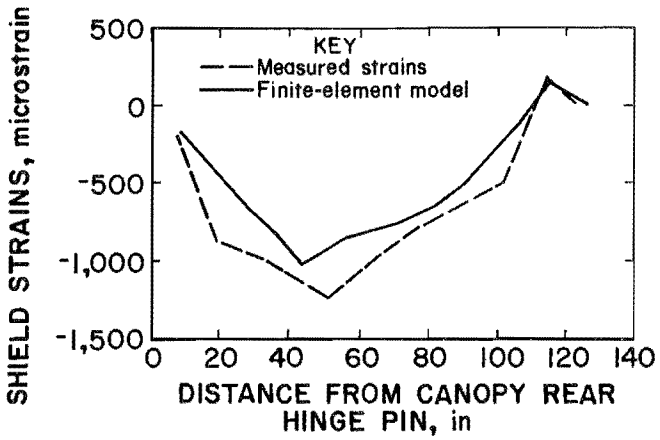

FIGURE 8.—Finite-element canopy pressure determinations.

CONCLUSIONS

An evaluation of shield mechanics can be accomplished either by rigid-body or elastic analysis of the shield structure. Rigid-body models assume all components remain rigid and do not deform during load application. Elimination of unknowns are required to produce a determinate solution of resultant shield loading by rigid-body static analysis of the shield structure. Tests in the MRS indicate two-dimensional rigid-body models can determine resultant vertical forces acting on the canopy to within 3 to 5 pct and resultant horizontal forces to within 25 pct or better depending on the load condition.

An elastic model with two degrees of freedom to account for the vertical (roof-to-floor) and horizontal (face-to-waste) displacement activity of the strata was also found to be an effective method of determining resultant forces acting on the shield canopy. In principle, the elastic solution should be more accurate providing the load-displacement relationship of the structure is properly defined. Test results indicate some nonlinearity in the shield stiffness, which makes an elastic solution more difficult. However, the elastic stiffness model did produce resultant force determinations comparable in accuracy with the rigid-body evaluations. The elastic model has the advantage of being able to isolate the direction of the strata displacement that produced the support reaction. In other words, horizontal support reaction produced in response to face-to-waste displacement can be isolated from horizontal reactions produced by roof-to-floor strata convergence. Ideally, a support would react only a vertical force to vertical displacements and a horizontal force to horizontal displacements. The shield structure, because of its geometry and mechanics, reacts both a vertical and horizontal force to uniaxial vertical and horizontal displacements, indicating the shield may be an inefficient design.

Ultimately, numerical solutions to shield mechanics will be the most beneficial in the evaluation of roof support structures. Currently, verifiable finite-element models have been difficult to produce, but the potential of the

finite-element technique is great. As additional experience is gained on how to effectively model longwall supports, improvement in the accuracy of the finite-element results will be realized. As advancements are made in modeling techniques, a goal will be to optimize the support structure by providing more efficient distribution of stresses in shield components. This could lead to considerable improvements in shield design with potential for a significant reduction in support costs.

REFERENCES

1. Peng, S. S. Longwall Mining. Wiley, 1984, pp. 239-259.

2. Peacock, A. Design of Shield Supports for the U.S. Coal Mine Industry. Paper in Proceedings of First Annual Conference on Ground Control in Mining (Morgantown, WV, July 27-29, 1981). WV Univ., 1981, pp. 174-185.

3. Barczak, T. M., and W. S. Burton. Three-Dimensional Shield Mechanics. BuMines RI 9091, 1987, 23 pp.

4. Barczak, T. M., and R. C. Garson. Shield Mechanics and Resultant Load Vector Studies. BuMines RI 9027, 1986, 43 pp.

5. Barczak, T. M., and S. J. Kravits. Shield-Loading Studies at an Eastern Appalachian Minesite. BuMines RI 9098, 1987, 81 pp.

6. Popov, E. P. Mechanics of Materials. Prentice-Hall, 1976, 421 pp.

7. Cook, R. D. Concepts and Applications of Finite Element Analysis. Wiley, 1981, pp. 1-20.

APPENDIX A.--DESCRIPTION OF MINE ROOF SIMULATOR

The Mine Roof Simulator (MRS) is a large hydraulic press (see figure 1 of text) designed to simulate the loading of full-scale underground mine roof supports. The MRS is unique in its abilities to apply both a vertical and a horizontal load simultaneously.

Both the vertical and horizontal axis can be programmed to operate in either force or displacement control. This capability permits tests, such as true friction-free controlled loading of shields, which cannot be accomplished in uniaxial test machines because the shield reacts a horizontal load to vertical roof convergence. Friction-free tests of this nature can be accomplished in the MRS by allowing the platen to float in the horizontal axis by commanding a zero horizontal load condition. Likewise, the MRS can apply controlled horizontal loading to a shield support; whereas, uniaxial test machines can only apply vertical loading with no control over horizontal load reactions or capability to provide a specified horizontal load to the structure. The controlled displacement capability allows determination of a structure's stiffness, which is essential to understanding the load-displacement characteristics of the structure.

The machine incorporates 20-ft square platens with a 16-ft vertical opening enabling full-scale testing of longwall support structures. Capacity of the simulator is 1,500 tons of vertical force and 800 tons of horizontal force and controlled displacement ranges of 24 in vertically and 16 in horizontally. Load and displacement control is provided in four ranges operating under a 12-bit analog-to-digital closed loop control network, providing a load control capability of better than 0.1 kip (100 lb) and displacement control capability of better than 0.001 in. in the smallest load-displacement range.

Machine control and data acquisition is achieved by a commercially available computer. Eighty-eight channels of test article transducer conditioning are proided. Data acquisition is interfaced with the control network so that machine behavior can be controlled by response of the test article instrumentation. For example, tests can be terminated or held when strain values reach a designated level in specified areas of the support structure. High-speed data acquisition is available with a separate computer at a rate of 300 samples per second. An X-Y-Z recorder provides real-time plotting of three data channels while all data are stored on computer disks for subsequent processing and analysis.

APPENDIX B.--THREE-DIMENSIONAL EQUATIONS OF EQUILIBRIUM

CANOPY

TABLE B-1. - Canopy nomenclature description

Symbol	Vector represented	Scalar components
$\tilde{P}$	Canopy hinge pin force	P_{x1}, P_{y1}, P_{z1}
$\tilde{Q}$	Canopy capsule force	Q_{x1}, Q_{y1}, Q_{z1}
$\tilde{L}$	Leg cylinder force	L_{x1}, L_{y1}, L_{z1}
$\tilde{R}$	Resultant force	R_{x1}, R_{y1}, R_{z1}
$\tilde{M}_P$	Canopy hinge pin moments	M_{Px1}, M_{Py1}, M_{Pz1}
$\tilde{M}_Q$	Canopy capsule moment	M_{Qx1}, M_{Qy1}, M_{Qz1}
$\tilde{M}_L$	Leg cylinder moment	M_{Lx1}, M_{Ly1}, M_{Lz1}
$\tilde{M}_R$	Canopy resultant force moment	M_{Rx1}, M_{Ry1}, M_{Rz1}
$\tilde{r}_Q$	Canopy capsule moment vector distance	x_{1Q}, y_{1Q} z_{1Q}
$\tilde{r}_L$	Leg cylinder moment vector distance	x_{1L}, y_{1L}, z_{1L}
$\tilde{r}_R$	Resultant moment vector distance	x_{1R}, y_{1R}, z_{1R}

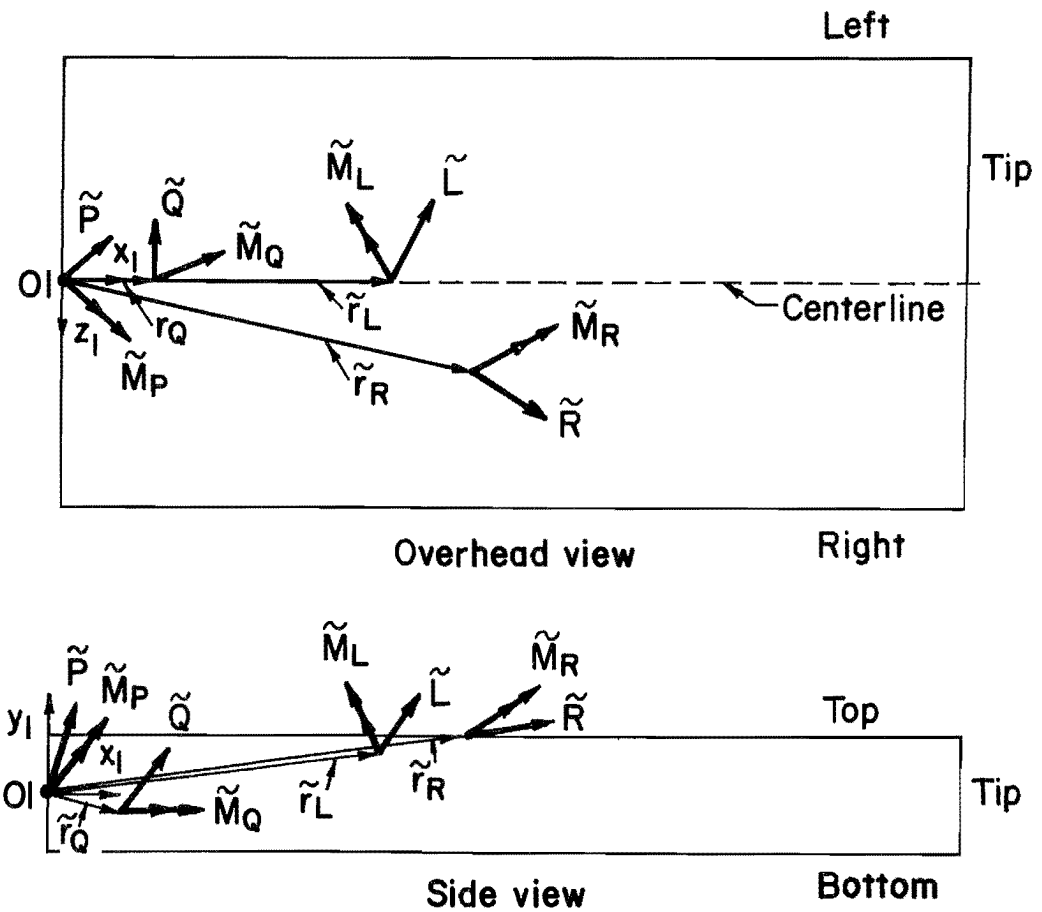

FIGURE B-1.—Three-dimensional free body diagram of canopy.

Summation of Forces (fig. B-1)

$$\sum\tilde{F} = \tilde{P} + \tilde{Q} + \tilde{L} + \tilde{R} = \tilde{0}. \tag{B-1}$$

$$\sum F_{x1} = P_{x1} + Q_{x1} + L_{x1} + R_{x1} = 0. \tag{B-2}$$

$$\sum F_{y1} = P_{y1} + Q_{y1} + L_{y1} + R_{y1} = 0. \tag{B-3}$$

$$\sum F_{z1} = P_{z1} + Q_{z1} + L_{z1} + R_{z1} = 0. \tag{B-4}$$

$$\sum\tilde{M}\ (01) = \tilde{M}_P + \tilde{M}_Q + \tilde{M}_L + \tilde{M}_R + (\tilde{r}_Q \times \tilde{Q}) + (\tilde{r}_L \times \tilde{L}) + (\tilde{r}_R \times \tilde{R}) = \tilde{0}. \tag{B-5}$$

$$\sum M_{x1}(01) = M_{Px1} + M_{Qx1} + M_{Lx1} + M_{Rx1} + (y_{1Q}Q_{z1} - z_{1Q}Q_{y1}) + (y_{1L}L_{z1} - z_{1L}L_{y1}) + (y_{1R}R_{z1} - z_{1R}R_{y1}) = 0. \tag{B-6}$$

$$\sum M_{y1}(01) = M_{Py1} + M_{Qy1} + M_{Ly1} + M_{Ry1} + (z_{1Q}Q_{x1} - x_{1Q}Q_{z1}) + (z_{1L}L_{x1} - x_{1L}L_{z1}) + (z_{1R}R_{x1} - x_{1R}R_{z1}) = 0. \tag{B-7}$$

$$\sum M_{z1}(01) = M_{Pz1} + M_{Qz1} + M_{Lz1} + M_{Rz1} + (x_{1Q}Q_{y1} - y_{1Q}Q_{x1}) + (x_{1L}L_{y1} - y_{1L}L_{x1}) + (x_{1R}R_{y1} - y_{1R}R_{x1}) = 0. \tag{B-8}$$

CAVING SHIELD

TABLE B-2. - Caving shield nomenclature description

Symbol	Vector represented	Scalar components
$\tilde{E}$	Canopy hinge pin force	E_{x2}, E_{y2}, E_{z2}
$\tilde{U}$	Capsule force	U_{x2}, U_{y2}, U_{z2}
$\tilde{T}$	Compression lemniscate link force	T_{x2}, T_{y2}, T_{z2}
$\tilde{S}$	Tension lemniscate link force	S_{x2}, S_{y2}, S_{z2}
$\tilde{R}_C$	Caving shield gob reaction force	R_{Cx2}, R_{Cy2}, R_{Cz2}
$\tilde{M}_E$	Canopy hinge pin moment	M_{Ex2}, M_{Ey2}, M_{Ez2}
$\tilde{M}_U$	Capsule moment	M_{Ux2}, M_{Uy2}, M_{Uz2}
$\tilde{M}_T$	Compression lemniscate link moment	M_{Tx2}, M_{Ty2}, M_{Tz2}
$\tilde{M}_S$	Tension lemniscate link moment	M_{Sx2}, M_{Sy2}, M_{Sz2}
$\tilde{M}_{RC}$	Gob reaction moment	M_{RCx2}, M_{RCy2}, M_{RCz2}
$\tilde{r}_E$	Canopy hinge pin moment vector distance	x_{2E}, y_{2E}, z_{2E}
$\tilde{r}_U$	Capsule moment vector distance	x_{2U}, y_{2U}, z_{2U}
$\tilde{r}_T$	Compression lemniscate link moment vector distance	x_{2T}, y_{2T}, z_{2T}
$\tilde{r}_{RC}$	Gob reaction moment vector distance	x_{2RC}, y_{2RC}, z_{2RC}

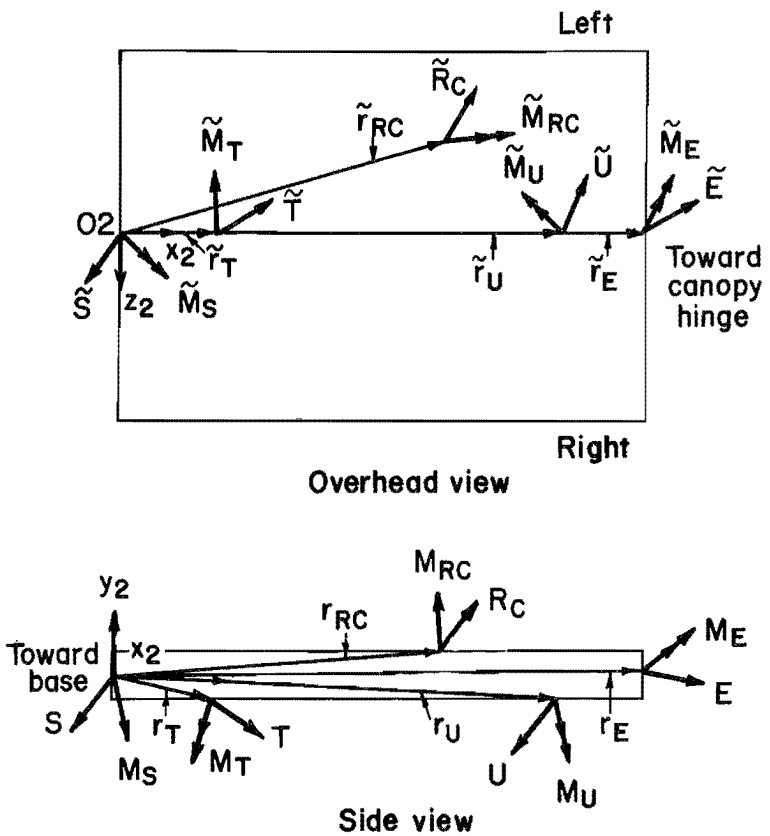

FIGURE B-2.—Three-dimensional free body diagram of caving shield.

Summation of Forces (fig. B-2)

$$\sum\tilde{F} = \tilde{E} + \tilde{U} + \tilde{T} + \tilde{S} + \tilde{R}_C = \tilde{0}. \tag{B-9}$$

$$\sum F_{x2} = E_{x2} + U_{x2} + T_{x2} + S_{x2} + R_{Cx2} = 0. \tag{B-10}$$

$$\sum F_{y2} = E_{y2} + U_{y2} + T_{y2} + S_{y2} + R_{Cy2} = 0. \tag{B-11}$$

$$\sum F_{z2} = E_{z2} + U_{z2} + T_{z2} + S_{z2} + R_{Cz2} = 0. \tag{B-12}$$

Summation of Moments (fig. B-2)

$$\sum\tilde{M}\ (02) = \tilde{M}_E + \tilde{M}_U + \tilde{M}_T + \tilde{M}_S + \tilde{M}_{RC} + (\tilde{r}_E \times \tilde{E}) + (\tilde{r}_U \times \tilde{U}) + (\tilde{r}_T \times \tilde{T}) + (\tilde{r}_{RC} \times \tilde{R}_C) = \tilde{0}. \tag{B-13}$$

$$\sum M_{x2}(02) = M_{Ex2} + M_{Ux2} + M_{Tx2} + M_{Sx2} + M_{RCx2} + (y_{2E}E_{z2} - z_{2E}E_{y2}) + (y_{2U}U_{z2} - z_{2U}U_{y2}) + (y_{2T}T_{z2} - z_{2T}T_{y2}) + (y_{2RC}R_{Cz2} - z_{2RC}R_{Cy2}) = 0. \tag{B-14}$$

$$\sum M_{y2}(02) = M_{Ey2} + M_{Uy2} + M_{Ty2} + M_{Sy2} + M_{RCy2} + (z_{2E}E_{x2} - x_{2E}E_{z2}) + (z_{2U}U_{x2} - x_{2U}U_{z2}) + (z_{2T}T_{x2} - x_{2T}T_{z2}) + (z_{2RC}R_{Cx2} - x_{2RC}R_{Cz2}) = 0. \tag{B-15}$$

$$\sum M_{z2}(02) = M_{Ez2} + M_{Uz2} + M_{Tz2} + M_{Sz2} + M_{RCz2} + (x_{2E}E_{y2} - y_{2E}E_{x2}) + (x_{2U}U_{y2} - y_{2U}U_{x2}) + (x_{2T}T_{y2} - y_{2T}T_{x2}) + (x_{2RC}R_{Cy2} - y_{2RC}R_{Cx2}) = 0. \tag{B-16}$$

BASE

TABLE B-3. - Base structure nomenclature description

Symbol	Vector represented	Scalar components
$\tilde{R}_B$	Base resultant reaction force.....	R_{Bx3}, R_{By3}, R_{Bz3}
$\tilde{B}$	Leg force.....	B_{x3}, B_{y3}, B_{z3}
$\tilde{C}$	Compression lemniscate link force.....	C_{x3}, C_{y3}, C_{z3}
$\tilde{D}$	Tension lemniscate link force.....	D_{x3}, D_{y3}, D_{z3}
$\tilde{r}_{RB}$	Base resultant reaction moment distance.....	x_{3RB}, y_{3RB}, z_{3RB}
$\tilde{r}_B$	Leg moment vector distance.....	x_{3B}, y_{3B}, z_{3B}
$\tilde{r}_C$	Compression lemniscate link moment distance.....	x_{3C}, y_{3C}, z_{3C}

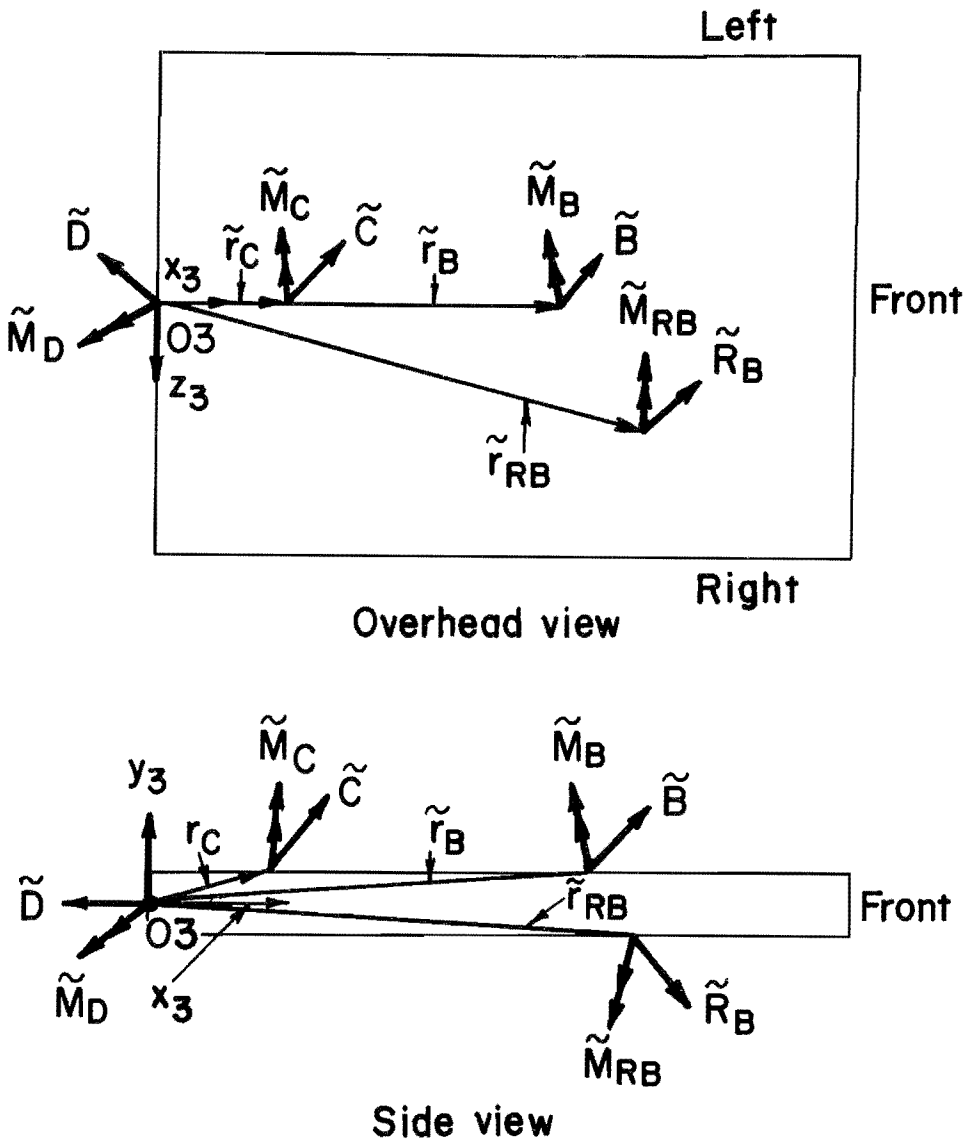

FIGURE B-3.—Three-dimensional free body diagram of base.

Summation of Forces (fig. B-3)

$$\sum\tilde{F} = \tilde{R}_B + \tilde{B} + \tilde{C} + \tilde{D} = \tilde{O}. \tag{B-17}$$

$$\sum F_{x3} = R_{Bx3} + B_{x3} + C_{x3} + D_{x3} = 0. \tag{B-18}$$

$$\sum F_{y3} = R_{By3} + B_{y3} + C_{y3} + D_{y3} = 0. \tag{B-19}$$

$$\sum F_{z3} = R_{Bz3} + B_{z3} + C_{z3} + D_{z3} = 0. \tag{B-20}$$

Summation of Moments (fig. B-3)

$$\sum M \quad (03) = \tilde{M}_{RB} + \tilde{M}_B + \tilde{M}_C + \tilde{M}_D + (\tilde{r}_{RB} \times \tilde{R}_B) + (\tilde{r}_B \times \tilde{B}) + (\tilde{r}_C \times \tilde{C}) = \tilde{O}. \tag{B-21}$$

$$\sum M_{x3}(03) = M_{RBx3} + M_{Bx3} + M_{Cx3} + M_{Dx3} + (y_{3RB}R_{Bz3} - z_{3RB}R_{By3}) + (y_{3B}B_{z3} - z_{3B}B_{y3}) + (y_{3C}C_{z3} - z_{3C}C_{y3}) = 0. \tag{B-22}$$

$$\sum M_{y3}(03) = M_{RBy3} + M_{By3} + M_{Cy3} + M_{Dy3} + (z_{3RB}R_{Bx3} - x_{3RB}R_{Bz3}) + (z_{3B}B_{x3} - x_{3B}B_{z3}) + (z_{3C}C_{x3} - x_{3C}C_{z3}) = 0. \tag{B-23}$$

$$\sum M_{z3}(03) = M_{RBz3} + M_{Bz3} + M_{Cz3} + M_{Dz3} + (x_{3RB}R_{By3} - y_{3RB}R_{Bx3}) + (x_{3B}B_{y3} - y_{3B}B_{x3}) + (x_{3C}C_{y3} - y_{3C}C_{x3}) = 0. \tag{B-24}$$

APPENDIX C.--TWO-DIMENSIONAL EQUATIONS OF EQUILIBRIUM

A simplistic, two-dimensional diagram of a generic two-legged shield support is shown in figure 2 in the text. The shield structure is an indeterminate structure with multiple load paths created by hydraulic leg and canopy capsule cylinders and the caving shield-lemniscate linkage system. Static equilibrium requirements can be reduced to three independent equations for solution of the vertical and horizontal resultant forces depicted in figure C-1. A static rigid-body analysis of the shield structure reveals that these equations can be developed by examining the forces acting on the canopy and canopy-caving shield combination by summation of moments about the canopy hinge pin, the instantaneous center of the lemniscate links, and the tension link and caving shield hinge pin; if the leg, canopy capsule, and compression lemniscate link forces are known. Simultaneous solution of these three independent equations provides generic solution to the resultant load vector parameters as follows.

$$VERT = (A + B + C - D + E - F - G) / (H - I), \qquad (C\text{-}1)$$

where

$$A = L^{*}COS\alpha * (X_6 - X_3) * CONS1,$$

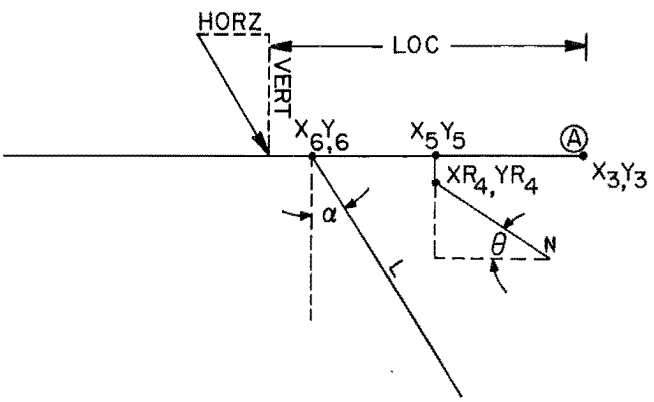

FIGURE C-1.—Summation of moments about canopy hinge pin.

$$B = N^{*}SIN\theta * (X_5 - X_3) * CONS1,$$

$$C = N^{*}COS\theta * (Y_5 - YR_4) * CONS1,$$

$$D = L^{*}COS\alpha * (X_6 - X_3) * CONS2,$$

$$E = L^{*}COS\alpha * (X_6 - X_1),$$

$$F = C^{*}COS\beta * (Y_2 - Y_1),$$

$$G = C^{*}SIN\beta * (X_2 - X_1),$$

$$H = (X_3 - X_1),$$

$$I = (X_3 - X_0) * CONS2,$$

$$CONS1 = (Y_3 - Y_1)/(Y_3 - Y_0) + 1,$$

$$CONS2 = (Y_3 - Y_1)/(Y_3 - Y_0),$$

and

$$HORZ = VERTLOC/(Y_3 - Y_0) + VERT * (X_3 - X_0)/(Y_3 - Y_0), - L^{*}COS\alpha * (X_6 - X_0)/(Y_3 - Y_0) + L^{*}SIN\alpha,$$

where

$$VERTLOC = L^{*}COS\alpha * (X_6 - X_3) + N^{*}SIN\beta * (X_5 - X_3) + N^{*}COS\beta * (Y_5 - YR_4),$$

$$MAGNITUDE = (VERT^2 + HORZ^2)^{1/2},$$

and

$$LOC = VERTLOC/VERT.$$

Interpretation of the terms are as follows:

VERT is the vertical shield reaction force,

HORZ is the horizontal shield reaction force,

L is the measured leg force,

N is the measured canopy capsule force,

C is the lemniscate link force determined from link strain measurements,

α is the leg angle relative to the vertical axis,

θ is the canopy capsule angle relative to the horizontal axis,

β is the lemniscate link angle relative to the horizontal axis, and

X_I, Y_I are spatial coordinates of the shield geometry.

Derivation of these equations is as follows:

1. Summation of moments about canopy hinge pin (fig. C-1)

$$\sum M(A)\curvearrowright + = -VERT * LOC + L * COS(\alpha) * (X_6 - X_3) + N * SIN(\theta)(X_5 - X_3) + N * COS(\theta) * (Y_5 - YR_4) = 0. \quad (C-2)$$

2. Summation of moments about instantaneous link center (fig. C-2)

$$\sum M(I)\curvearrowright + = -VERT * \{LOC + (X_3 - X_0)\} + HORZ * (Y_3 - Y_0) + L * COS(\alpha) * (X_6 - X_0) - L * SIN(\alpha) * (Y_3 - Y_0) = 0. \quad (C-3)$$

3. Summation of moments about tension link and caving shield hinge pin (fig. C-3)

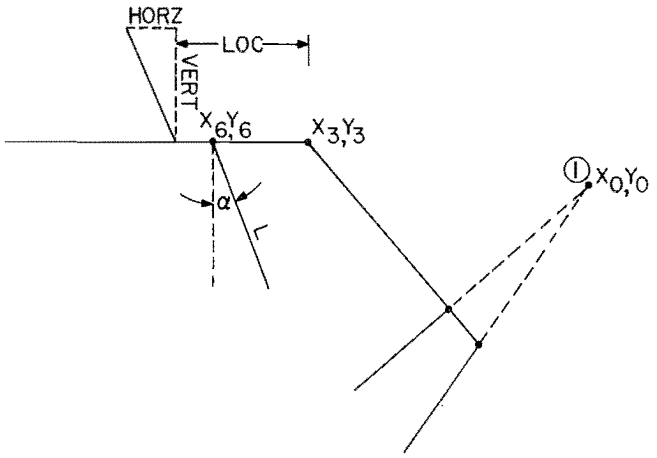

FIGURE C-2.—Summation of moments about instantaneous lemniscate link center.

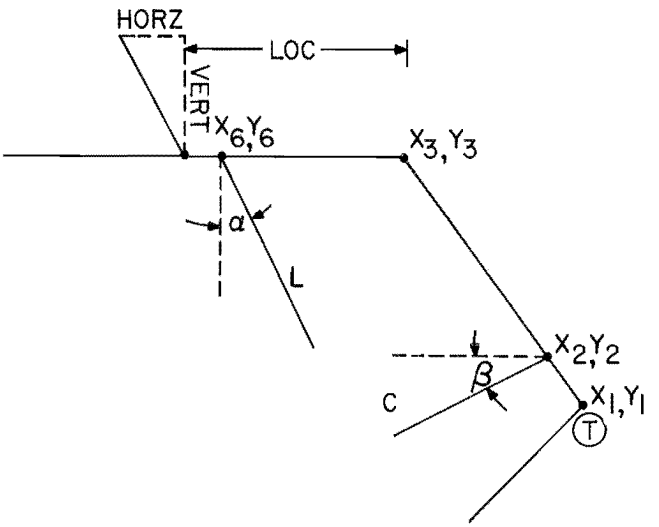

FIGURE C-3.—Summation of moments about tension link and caving shield hinge pin.

$$\sum M(T)\curvearrowright + = -VERT * \{LOC + (X_3 - X_1)\} + HORZ * (Y_3 - Y_1) + L * COS(\alpha) * (X_6 - X_1) - L * SIN(\alpha) * (Y_3 - Y_1) - C * COS(\beta) * (Y_2 - Y_1) - C * SIN(\beta) * (X_2 - X_1) = 0. \quad (C-4)$$

Solution of these equations is as follows:

Step 1. Solve equation C-3 for HORZ:

$$HORZ = [VERT * \{LOC + (X_3 - X_0)\} - L * COS(\alpha) * (X_6 - X_0) + L * SIN(\alpha) * (Y_3 - Y_0)] / (Y_3 - Y_0).$$

Step 2. Solve equation C-2 for VERT * LOC:

$$VERT * LOC = L * COS(\alpha) * (X_6 - X_3) + N * SIN(\theta) * (X_5 - X_3) + N * COS(\theta) * (Y_5 - YR_4).$$

Step 3. Substitute VERT * LOC from step 2 and HORZ from step 1 into equation C-4 and solve for VERT, yielding equation C-1.

Step 4. Substitute VERT * LOC from step 2 and VERT from step 3 into equation C-2 to determine HORZ

$$HORZ = VERT * LOC/(Y_3 - Y_0) + VERT * (X_3 - X_0)/(Y_3 - Y_0) - L * COS(\alpha) * (X_6 - X_0) / (Y_3 - Y_0) + L * SIN(\alpha).$$

Step 5. Solve equation from step 2 for LOC

$$LOC = VERT * LOC / VERT.$$

APPENDIX D.--SHIELD STIFFNESS DETERMINATIONS

The load-displacement relationship of the shield structure can be described by the following mathematical relationship, which describes vertical and horizontal support reactions as a function of vertical (roof-to-floor) and horizontal (face-to-waste) displacements.

$$F_v = K_1\delta_v + K_2\delta_h \qquad (D\text{-}1)$$

and

$$F_h = K_3\delta_v + K_4\delta_h \qquad (D\text{-}2)$$

where F_v = resultant vertical force,

F_h = resultant horizontal force,

δ_v = vertical (roof-to-floor) shield displacement,

δ_h = horizontal (face-to-waste) shield displacement,

and

K_1, K_2, K_3, K_4 = shield stiffness coefficients.

The shield stiffness coefficients (K_1, K_2, K_3, K_4) were determined with the aid of the Bureau's Mine Roof Simulator (MRS). A description of the MRS and its capabilities is provided in appendix A. The simulator is active in both the vertical and horizontal axis and can be programmed to operate in displacement control independently in each axis, allowing a shield to be subjected to controlled vertical and horizontal displacements.

Examination of equations D-1 and D-2 and figures D-1 and D-2 reveals how the shield stiffness parameters were determined. By commanding the MRS to maintain a fixed horizontal displacement of the platen (fig. D-1), the shield is subjected to pure vertical convergence. Terms $K_2\delta_h$ and $K_4\delta_h$ of equations D-1 and D-2, respectively, then become zero since $\delta_h = 0$, leaving $F_v = K_1\delta_v$ and $F_h = K_3\delta_v$. From the vertical shield displacement and the associated reactive forces of the shield, the vertical stiffness parameters (K_1 and K_3) can be calculated: K_1 being equal to the ratio of resultant vertical shield load to the vertical displacement and K_3 equal to the ratio of the resultant horizontal load to the vertical displacement. Likewise, subjecting the shield to pure horizontal (face-to-waste) displacement (fig. D-2) permits determination of stiffness parameters K_2 and K_4 as terms $K_1\delta_v$ and $K_3\delta_v$ of equations D-1 and D-2, respectively, become zero for $\delta_v = 0$.

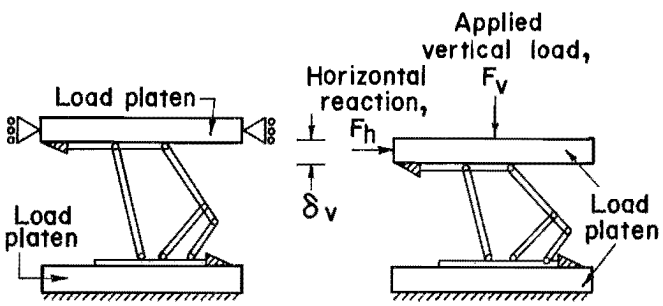

$F_v = K_1\delta_v + K_2\delta_h \rightarrow \delta_h = 0 \rightarrow F_v = K_1\delta_v$

$F_h = K_3\delta_v + K_4\delta_h \rightarrow \delta_h = 0 \rightarrow F_h = K_3\delta_v$

FIGURE D-1.—Vertical convergence tests in MRS.

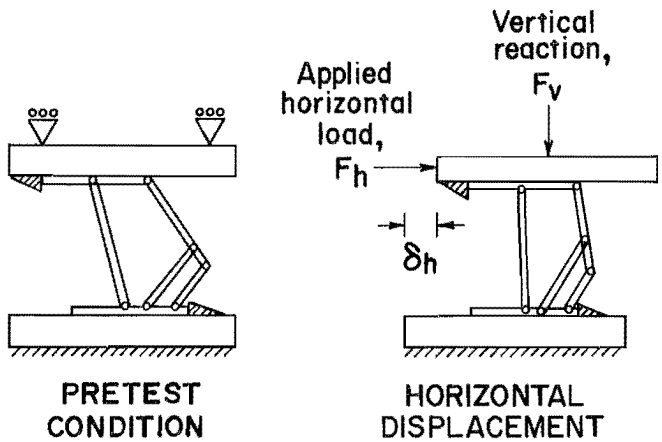

$F_v = K_1\delta_v + K_2\delta_h \rightarrow \delta_v = 0 \quad F_v = K_2\delta_h$

$F_h = K_3\delta_v + K_4\delta_h \rightarrow \delta_v = 0 \quad F_h = K_4\delta_h$

FIGURE D-2.—Horizontal displacement tests in MRS.

The results of the MRS tests for one shield configuration are shown in figure 4 in the text, depicting reactive forces as a function of applied MRS displacements. The slopes of the force-displacements plots under controlled vertical and horizontal convergence determine the stiffness parameters (K_1, K_2, K_3, K_4). Table D-1 presents least squares analyses determinations of the stiffness parameters at shield heights of 58 and 78 in, with and without an active canopy capsule. As can be seen from the table, the shield exhibits different responses at different shield heights because of changes in the geometry of the structure. Generally speaking, the stiffness of the structure in both the vertical and horizontal axis increases at reduced shield heights. This necessitates developing characteristic stiffness curves as a function of shield height.

TABLE D-1. - Shield stiffness parameters, kips per inch

Shield configuration	K_1	K_2	K_3	K_4
78 in:				
Active capsule.....	585	174	157	203
Inactive capsule...	633	268	228	229
58 in:				
Active capsule.....	666	505	328	505
Inactive capsule...	715	517	430	378

U.S. GOVERNMENT PRINTING OFFICE: 1987 - 605-017/60124

INT.-BU.OF MINES,PGH.,PA. 28611